THE JOURNAL OF PHYSICAL CHEMISTRY C
A JOURNAL OF THE AMERICAN CHEMICAL SOCIETY

pubs.acs.org/JPCC

Article

Decoupling Chemically Active 2D Molecular Overlayers from the Substrate: Chlorophenyl Porphyrins on Graphene/Ir(111)

Duncan John Mowbray, Alejandro Pérez Paz, Rodrigo C. C. Ferreira, Valeria Milotti, Pedro Schio, Wendell Simoes e Silva, Thomas Pichler, Abner de Siervo,* and Juan Carlos Moreno-López*

Cite This: J. Phys. Chem. C 2023, 127, 8751−8758

Read Online

ACCESS | Metrics & More | Article Recommendations | Supporting Information

ABSTRACT: The synthesis of atomically precise chemically active 2D molecular overlayers may be hindered by chemical interactions with the underlying substrate, especially when based on chlorophenyl porphyrins. At the same time, the chlorination of graphene, i.e., the covalent bonding of chlorine atoms with sp^2 carbon atoms, is known to have a significant influence on the electronic properties of pristine graphene. In this study, we deposit a chlorinated porphyrin molecule, namely 5,10,15,20-tetrakis(4-chlorophenyl)porphyrin (Cl_4TPP), on graphene/Ir(111). Employing a combined experimental and theoretical approach, we demonstrate that the porphyrin layer physisorbed on graphene self-assembles into a periodic square-like arrangement. This carpet-like growth is unperturbed by the step edges of the substrate, neither in its periodicity nor in its orientation. In addition, the molecular overlayer is thermally stable and does not alter the electronic properties of graphene. Remarkably, we show that Cl_4TPP does not experience a dechlorination reaction with the underlying substrate, even after postdeposition annealing temperatures as high as 550 K. Moreover, postdeposition annealing at 700 K suggests the Cl_4TPP molecules desorb intact without affecting graphene's electronic properties. In so doing, we demonstrate the effectiveness of graphene physisorbed on Ir(111) to both promote the formation and preserve the properties of chemically reactive 2D overlayers based on chlorophenyl porphyrins. These results show physisorbed graphene's potential as a general templating material for the formation of highly reactive self-assembled 2D overlayers.

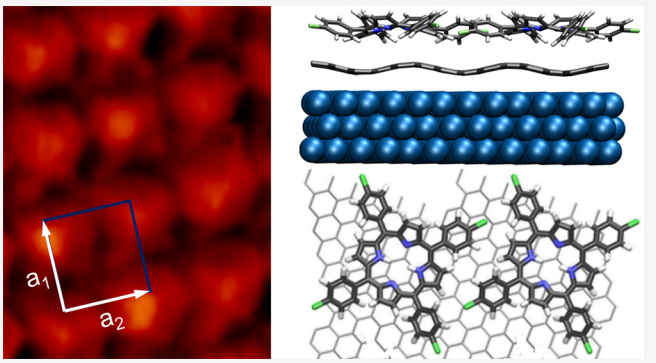

1. INTRODUCTION

Over the past few years, a significant number of scientific publications and patents have paved the way toward the commercial realization of graphene-based electronic devices, including spin filters and giant magnetoresistance devices,[1−4] tunable terahertz devices,[5−7] or high-frequency large-bandwidth electronics,[8−11] to mention just a few. In addition, molecular self-assembly has emerged as a feasible and scalable route toward the realization of graphene−molecule devices with tailored properties to expand the scope of their magnetic/electronic applications.[12−16] Magnetic porphyrin molecules covalently bonded or "wired" to graphene nanoribbons have been proposed as potential molecular spintronic systems. However, to exploit their intrinsic magnetic properties, it is necessary to decouple their spin-carrying orbitals from the metallic surface, for instance, by lifting with an STM tip.[16] This approach, however, is not scalable to 2D overlayers. To some extent, graphene can be considered an inert substrate that may partially decouple organic molecules from any underlying metallic substrate.[17−19] This relative inertness of graphene, together with its potential to provide an atomically flat surface, makes it an ideal candidate buffer layer for conserving the pristine physicochemical properties of self-assembled 2D molecular overlayers. However, the vast range of molecular adsorbates requires a clear strategy to rationalize the subtle interplay between intermolecular forces and molecule−graphene interactions. This can potentially have a massive influence on the electronic and optical properties of both the molecular overlayer and graphene. In this regard, particular attention has to be placed on chlorine-containing molecules due to the covalent reaction of chlorine atoms with sp^2 carbon atoms[20−24] and the plausible intercalation of metal chlorides between graphene and the metal substrate.[25−27] Chlorine atoms and chlorine-containing metals can significantly influence the electronic properties of graphene. Graphene chlorination can open an electronic bandgap of around 1.2 to 1.7 eV[20,28,29] and decrease the Fermi velocity and carrier

Received: January 11, 2023
Revised: April 13, 2023
Published: April 28, 2023

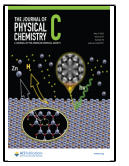

mobility, μ.[22,30] However, the latter may be a drawback for some graphene-based applications, e.g., in high-frequency devices.[31] For this reason, further progress is required to better understand the interaction of adsorbed molecules with graphene substrates, especially in the case of chlorine-containing molecules. Such work will help to selectively tailor graphene's electronic properties, open the possibility of using graphene as an inert surface for molecular self-assembly where the electronic and optical properties of the molecular overlayer remain unperturbed, and perform on-surface reactions controlled by external means such as temperature, light, or the postdeposition of catalytic adatoms.

In this paper, we present a combined experimental and computational study of the adsorption of a molecular layer of chlorinated porphyrins, namely 5,10,15,20-(tetra-4-chlorophenyl)porphyrin (Cl_4TPP), on a marginally p-doped graphene/Ir(111) surface. Using a combined scanning tunneling microscopy (STM), low-energy electron diffraction (LEED), and density functional theory (DFT) approach, we can rationalize the molecular self-assembly of Cl_4TPP on graphene/Ir(111). By comparing our X-ray photoelectron spectroscopy (XPS) and angle-resolved photoemission spectroscopy (ARPES) measurements, we characterize the binding energies of the different molecular components and study the influence of the organic layer on the electronic properties of graphene in the vicinity of the Dirac point. Our results show that the electronic properties of graphene remain unaltered. Specifically, no change in XPS binding energies, no doping, or change in the Fermi velocity are observed. This work not only highlights the relevance of Cl_4TPP as a thermally stable physisorbed organic layer on graphene but also directly shows its influence, or lack thereof, on the electronic properties of pristine graphene.

2. METHODS

2.1. Experimental Details. The experiments were performed in two different ultrahigh-vacuum (UHV) systems: an STM/XPS system at UNICAMP equipped with a scanning tunneling microscope (STM) operating at 5×10^{-11} mbar and an STM/XPS system installed in the PGM beamline (Planar Grating Monochromator) at the Brazilian Synchrotron Light Laboratory (LNLS) equipped with an ARPES Specs Phoibos 150 analyzer, an STM, and a LEED, among other facilities.

The Ir(111) single crystal was cleaned by several cycles of Ar^+ sputtering (1200 V at 5 μA cm^{-2}) for 60 min with subsequent annealing at 1575 K for 10 min. Graphene was grown by the chemical vapor deposition (CVD) method by keeping the sample at 1575 K while ethylene (99.99%) gas was introduced into the chamber at a pressure of 6×10^{-7} mbar. The pristine graphene sample was transferred to the PGM beamline with air exposition for approximately an hour and posterior annealed at 700 K under UHV conditions to remove atmospheric adsorbates (e.g., water). The feasibility of this method to obtain graphene samples has been demonstrated in the literature.[32−34] Cl_4TPP molecules were deposited in situ in the PGM beamline, using a Knudsen cell kept at a temperature of about 570 K, whereas the sample was kept at room temperature. Two independent SPECS Aarhus 150 STM microscopes were used for this work: one at UNICAMP and another at the PGM beamline. The STM measurements were performed in constant current mode with tungsten tips cleaned in situ by Ar^+ sputtering. All the STM measurements were performed at room temperature. STM bias voltages were applied to the sample, and the images were analyzed using the WSXM software.[35]

The XPS measurements with synchrotron light were performed at the PGM Beamline of LNLS[36] in normal emission, with a pass energy of 10 eV and photon energy of $h\nu$ = 400 eV. All photoemission peaks were fitted with a Doniach−Sunjic form convoluted with a Gaussian profile. The binding energy of the spectra was calibrated by setting the Ir $4f_{7/2}$ bulk and surface components to previously reported values.[37−40] The Doniach−Sunjic shape is characterized by a Lorentzian width, which takes into account the finite core−hole lifetime, and by the asymmetry parameter α that describes low-energy electron−hole pair excitations close to the Fermi level. The Gaussian distribution describes instrumental broadening, phonon contributions, and sample inhomogeneities. The inelastic background contribution of the spectra was removed by Shirley backgrounds.[41] After a Shirley background subtraction,[41] the C 1s spectra were fitted using a set of two Doniach−Sunjic peaks characterized by a Lorentzian width γ = 0.21 eV and an asymmetric parameter α = −0.01 convoluted with a small Gaussian contribution. The Cl 2p spectra have been fitted using Doniach−Sunjic lines characterized by a Lorentzian width γ = 0.46 eV and an asymmetric parameter α = −0.10.

The ARPES measurements were performed at a sample temperature of 61 K with a photon energy of $h\nu$ = 102.4 eV. At this photon energy, the π-band of graphene is expected not to diminish its photoemission intensity close to the Fermi energy E_F.[42,43] At this point, it is worth highlighting our experiments' energy and angular resolution. At 61 K the energy resolution, including thermal broadening contribution, is ∼40 meV with an angular resolution of 0.1°.

2.2. Computational Details. DFT calculations were performed using a linear combination of atomic orbitals (LCAOs)[44] to represent the Kohn−Sham (KS) wave functions within the projector-augmented wave method (PAW)[45] code GPAW.[46] Double-ζ-polarized (DZP) basis sets were used for all atomic species to represent the KS wave functions. We employed Perdew, Burke, and Ernzerhof's (PBE)[47] implementation of the generalized gradient approximation (GGA) for the exchange and correlation (xc) functional and Grimme's semiempirical correction (PBE-D3)[48] to describe van der Waals (vdW) interactions at the D3 level. We used a grid spacing of $h \approx 0.2$ Å, a $1 \times 3 \times 1$ k-point sampling, and an electronic temperature of k_BT = 0.1 eV extrapolating all energies to $T \to 0$ and performed structural relaxation of the adsorbed species until a maximum force $F_{max} \lesssim 0.03$ eV/Å was obtained. To model the Cl_4TPP overlayer on the graphene/Ir(111) surface, we employ two Cl_4TPP molecules and a 7×6 orthogonal graphene overlayer relaxed on a three-layer Ir frozen slab of 68 atoms per layer in a supercell of $28.736 \times 15.118 \times 25$ Å^3 with $\theta = 92°$, generated using Ir's experimental lattice parameter (a = 3.84 Å), with more than 11 Å of vacuum between repeated images. This supercell for the Cl_4TPP overlayer on graphene/Ir(111) is commensurate to that found in ref 49 for Cl_4TPP on Ag(111) and is only slightly compressed (∼5%) relative to our STM measurements (30.4×15.8 Å^2). Bader charge transfer[50] between the Cl_4TPP overlayer, graphene, and Ir(111) was calculated using the PAW all-electron charge density as input to the BADER code.[51] STM simulations have employed the Tersoff−Hamann approximation[52] in constant-current mode with a bias of U =

https://doi.org/10.1021/acs.jpcc.3c00235
J. Phys. Chem. C 2023, 127, 8751−8758

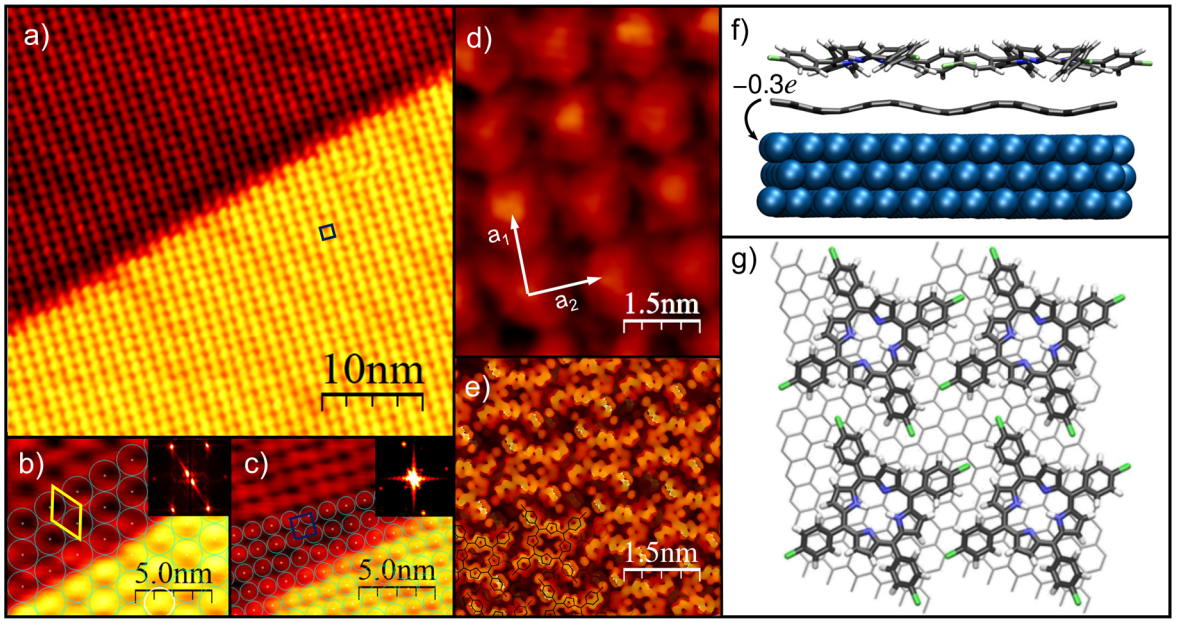

Figure 1. (a) STM image of Cl_4TPP on graphene/Ir(111) ($A = 45 \times 40$ nm^2, $U = -1.7$ V, $I = 0.09$ nA). (b) Graphene on Ir (111). A careful inspection reveals a shift of the Moiré pattern over the step edge. (c) Cl_4TPP on graphene/Ir(111) with the molecular layer showing continuity over the step edge. Insets show the 2D-FFT of the STM images (b) and (c). (d) STM image of Cl_4TPP on graphene/Ir(111) ($A = 5 \times 3.6$ nm^2, $U = +1.7$ V, $I = 0.65$ nA). (e) DFT simulated STM image of the relaxed square-like network. (f) Side and (g) top view of the DFT relaxed structure of Cl_4TPP on graphene/Ir(111) showing the charge transfer of $-0.3e$ from graphene to Ir(111). C, H, N, Cl, and Ir atoms are marked in gray, white, blue, green, and indigo, respectively. The Ir(111) atoms were omitted for clarity in (g).

+1.7 V relative to the Fermi level as implemented in the code ASE.[53]

To determine the molecular overlayer's total energy dependence on the substrate's lattice parameters, we performed calculations for the Cl_4TPP overlayer in a vacuum, stretching the unit cell parameter by up to 7.5% in steps of 0.5%. To reduce any dependence on the calculations' grid spacing, these calculations were instead performed using a plane-wave (PW) representation for the KS wave functions, with a plane-wave cutoff of $E_{cut} = 600$ eV, as implemented in GPAW.[46]

3. RESULTS AND DISCUSSION

Before depositing Cl_4TPP molecules, the graphene surface was carefully characterized. STM images show a uniform Moiré pattern superstructure unperturbed over extended areas of the Ir(111) substrate, as shown in Figure S1. From the STM images, the periodicity of the Moiré superstructure is determined to be 9 times the interatomic distance on Ir(111) with the $[11\bar{2}0]_{gr}$ direction of graphene aligned along the $[1\bar{1}0]_{Ir}$ direction of iridium.[54] These results are in excellent agreement with LEED experiments, where the satellite spots from the Moiré pattern can be observed around the Ir(111) hexagonal spots (see Figure S1). The well-defined spots in the LEED pattern suggest long-range order over extended zones of the surface. The excellent agreement between LEED and STM measurements, both in the periodicity and in the orientation of the graphene layer over the Ir(111) surface, allows us to identify the graphene layer as the so-called R0 graphene unambiguously.[54−56]

Next, Cl_4TPP molecules were deposited on graphene/Ir(111) held at room temperature. STM images show a periodic square arrangement of bright protrusions over the surface (see Figure 1a). The unit cell parameters are determined to be $a_1 = 15.2$ Å, $a_2 = 15.8$ Å, and $\theta = 92 \pm 1°$. By comparing this unit cell with the size of an individual molecule in the gas phase ($a_1 = 13.4$ Å, $a_2 = 13.6$ Å),[57] it is clear that only one molecule per unit cell is allowed within this configuration. This unit cell is incommensurate and breaks the triangular symmetry of both layers underneath, i.e., the graphene and the Ir(111) surface, suggesting a relatively weak molecule−substrate interaction.

A careful analysis of the STM images at the step-edge of the substrate shows an important difference between the growth of the molecular layer and graphene. On the one hand, graphene shows a displacement of the Moiré periodicity over the step edges of the substrate. On the other hand, the molecular layer remains unperturbed at both sides of the step edges. Figure 1b shows a step edge of graphene on Ir(111) where a green hexagonal lattice has been superimposed. While in the upper terrace (bottom-right corner) the Moiré spots are placed inside the superimposed lattice, in the lower terrace the Moiré spots are shifted outside the superimposed lattice. This shift originates from a subtle displacement between the graphene overlayer and the metal surface; i.e., a 0.2715 nm displacement of the graphene layer in the $[1\bar{1}0]_{Ir}$ direction gives rise to an amplified Moiré pattern displacement of $t \approx 2.5$ nm.[54] Figure 1c shows that the Cl_4TPP pattern remains unperturbed on both sides of the step edges; i.e., all the Moiré spots are inside the superimposed lattice on both the upper and lower terraces.

To gain additional insight into the driving force of the molecular self-assembly, a partially submolecular resolved STM image of Cl_4TPP on graphene/Ir(111) is shown in Figure 1d, where individual molecules are imaged as a protrusion with diagonal rod-like structures pointing toward neighboring molecules. However, it is worth remembering that the local density of states (LDOS), measured in STM images, is a convolution of geometric and electronic contributions from the

https://doi.org/10.1021/acs.jpcc.3c00235
J. Phys. Chem. C 2023, 127, 8751−8758

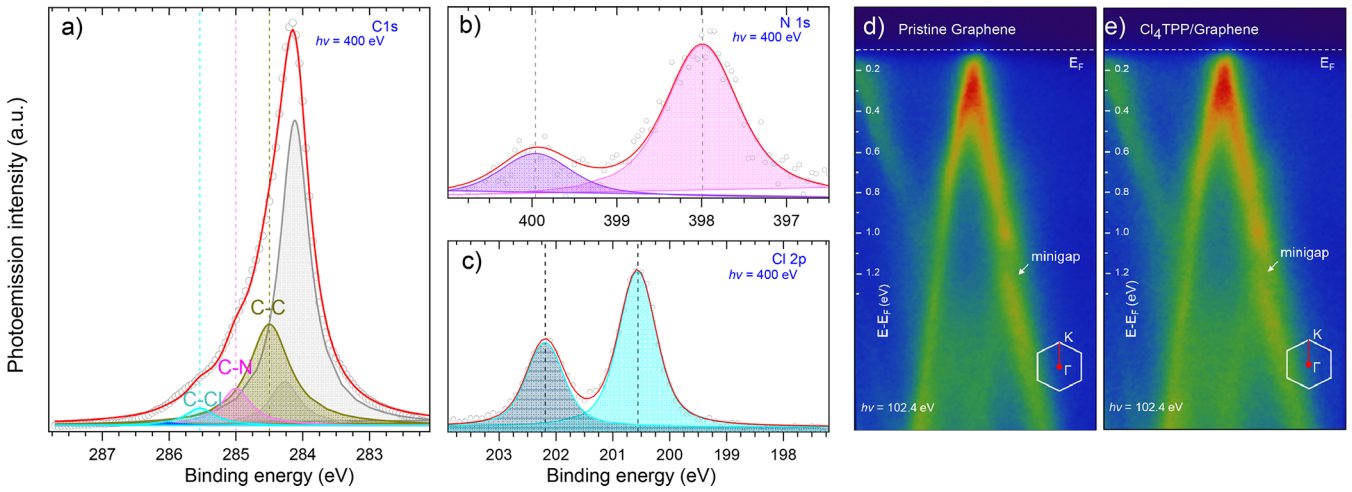

Figure 2. Photoemission spectra. XPS measurements of Cl_4TPP on graphene/Ir(111): (a) C 1s spectrum; (b) Cl 2p spectrum. (c) N 1s spectrum. Each component fit and the Shirley background line are depicted in the XPS images. ARPES measurements of (d) pristine graphene/Ir(111) and (e) Cl_4TPP on graphene/Ir(111).

tip and sample,[58] so the interpretation of this image is not straightforward. To better rationalize our results, we have performed DFT calculations of a Cl_4TPP molecular overlayer[49] adsorbed on the graphene/Ir(111) surface. First, we adsorbed a graphene atomic layer on a three-layer Ir(111) slab, relaxing the graphene until the most energetically favorable configuration was obtained. As a result, the graphene layer shows a mean height of 0.337 nm above the Ir(111) surface and a corrugation of around ±0.04 nm (cf. Figure 1f). This is in excellent agreement with X-ray standing wave (XSW) experiments, where a mean height of 0.338 ± 0.04 nm[59,60] was reported. The mean height is almost equal to the interlayer distance observed for bulk graphite (0.336 nm), suggesting a relatively weak interaction, i.e., physisorption, of the graphene layer on the Ir(111) substrate. Next, we placed the Cl_4TPP overlayer on the relaxed graphene/Ir(111) surface, allowing the molecules to relax. Figures 1e,f,g show the STM simulated image of our relaxed DFT molecular network,and the side and top views of our relaxed atomic structures, respectively. Figure 1e shows that the overall structure of the molecules is parallel to the surface, in good agreement with the so-called saddle structure of porphyrin molecules.[49,61−64] Specifically, we find the distances between terminal Cl atoms of the Cl_4TPP overlayer on graphene/Ir(111) are 12.9 and 14.0 Å along the hydrogenated and dehydrogenated pyrrole directions, respectively. This is only somewhat more rectangular than Cl_4TPP's 13.4 × 13.6 $Å^2$ area in the gas phase,[57] another indicator of physisorption. From our DFT supercell, we obtain unit cell parameters of a_1 = 14.368 Å, a_2 = 15.118 Å, and θ = 92° per Cl_4TPP molecule of the overlayer, in good agreement with our STM measurements (see Computational Details for further details). Furthermore, the DFT unit cell is ∼5% compressed relative to the experimental cell in order to ensure we have a unit cell that is commensurate with the Ir substrate. The fact that this is not the case experimentally, i.e., the unit cell of the Cl_4TPP overlayer is incommensurate with the Ir(111) surface, is yet another indicator of physisorption.

Both our STM experiments and DFT calculations suggest the interactions between the Cl_4TPP molecular overlayer, graphene, and the Ir(111) substrate are all relatively weak. To study the influence of the substrate on the molecular conformation, we also performed DFT calculations for the relaxed Cl_4TPP overlayer in a vacuum, while stretching the supercell parameters by more than 7.5%, i.e., ranging between those of Ir(111) and Ag(111). Remarkably, our DFT simulations show that the molecule overlayer could easily accommodate this stretching, with all changes in the total energy of the system within the accuracy of our DFT calculations (±50 meV). This suggests molecular interactions within the overlayer are rather "soft", long-ranged, and insensitive to the substrate's geometry or any corrugation. These results highlight the key role played by molecule−molecule interactions in stabilizing the molecular network. In this regard, our DFT relaxed structures show C−Cl···H−C hydrogen bonds ($d_{Cl\cdots H} \approx$ 2.5 to 2.9 Å) between chlorine atoms and phenyl groups of neighboring molecules, as the main stabilizing force. We also find at the PBE GGA level[47] that the Cl_4TPP overlayer on graphene/Ir(111) is 0.37 eV/molecule more stable than the molecular overlayer in gas phase, consistent with physisorption.

We performed photoemission experiments to gain additional insight into the chemical environments of the graphene and Cl_4TPP molecules. At this point, it is worth highlighting that the Ir 4f spectrum has been fitted using a set of two Doniach−Sunjic peaks characterized by a Lorentzian width Γ = 0.20−0.25 eV and an asymmetric parameter α = −0.05 to acknowledge the contributions from its bulk and surface components (see Figure S2). For this reason, whereas the bulk components are centered at 60.78 eV (Ir $4f_{7/2}$) and 63.80 eV (Ir $4f_{5/2}$), the surface components have peaks centered at 60.25 and 63.29 eV, in agreement with previously reported works.[37−40] This fitting allows us to monitor potential changes in the chemical environment of both bulk and surface iridium atoms. The unmodified presence of the Ir 4f surface component shows that the iridium surface is unaffected by the graphene layer.[32,37,65] Similarly, a set of two components has been used to fit the C 1s XPS contribution of graphene to acknowledge the heterogeneous modulation of the carbon atoms originating from the Moiré pattern (see Figure S3). While the carbon atoms placed in the Moiré's hills have a weaker interaction with the Ir substrate than those placed in the Moiré's valley, a difference in binding energies is expected. For this reason, our C 1s spectrum of clean graphene/Ir(111) shows components centered at 284.12 and 284.27 eV with a

https://doi.org/10.1021/acs.jpcc.3c00235
J. Phys. Chem. C 2023, 127, 8751−8758

ratio of 7:1, in agreement with reported values for monolayer graphene on Ir(111).[37,66]

Next, we performed photoemission experiments after depositing one monolayer of Cl_4TPP molecules on our previously characterized graphene/Ir(111) surface. Figure 2a shows the C 1s spectrum once Cl_4TPP molecules are deposited on graphene. Here, besides the C 1s XPS contribution of graphene (gray fit), three additional components are needed to account for the contribution of the molecular Cl_4TPP layer. These peaks are centered at 284.50, 285.00, and 285.54 eV and are ascribed to C−C, C−N, and C−Cl, respectively.

Taking into account the density of carbon atoms in both graphene and the molecular network, 38.2 and 17.9 atoms/nm^2, respectively, the C 1s integrated areas of graphene and one complete monolayer of Cl_4TPP molecules are expected to show a ratio of ≈2.1:1 (without considering the attenuation of the graphene's XPS signal due to the molecular layer). Our XPS fitting shows a graphene/molecule C 1s ratio of 1.9:1, in good agreement with the expected value for an almost complete monolayer of Cl_4TPP molecules on graphene.

Now we will focus on the N 1s and Cl 2p contributions from the Cl_4TPP molecular overlayer. Aminic and iminic nitrogens of the molecule show components centered at 397.95 and 399.99 eV, respectively. The Cl 2p spectrum is characterized by two components, corresponding to Cl $2p_{3/2}$ and Cl $2p_{1/2}$, with a spin−orbit splitting of 1.6 eV. These components have a binding energy of 200.59 and 202.20 eV ± 0.03 eV, in excellent agreement with reported values for Cl_4TPP and chlorobenzene molecules.[49,57,67] This result shows that no dechlorination of Cl_4TPP molecules is detected after room temperature deposition on graphene. This is in clear contrast with the reported dechlorination observed after room temperature deposition of Cl_4TPP direct on metallic substrates, i.e., 40% dechlorination on Cu(111)[57] and 6% on Ag(111).[49] Moreover, on Cu(111) the reaction is barrierless, and after 24 h at room temperature, 100% dechlorination has been observed.[57] Overall, this tells us that Cl_4TPP interacts strongly with metal surfaces, especially those that the d-band model[68] predicts to be more strongly binding than Ag(111), such as Ir(111). Furthermore, even after postdeposition annealing at temperatures as high as 550 K, no dechlorination of Cl_4TPP is observed, neither in the C 1s/Cl 2p XPS spectra (see Figure S4) nor as changes in the STM images of the molecular networks. At this point, it is worth highlighting that if dechlorination occurred, we would expect a decrease in the intermolecular distance, resulting in an STM-measurable decrease of the unit cell parameters. In fact, reported results for 5,10,15,20-tetraphenyl-21*H*,23*H*-porphyrin (H_4TPP) molecules on graphene found a unit cell 10% smaller than the one reported by us,[69] adding further support for our observations. Postdeposition annealing at 700 K suggests that desorption of Cl_4TPP molecules occurs without dechlorination and without affecting the C 1s peak position of graphene (see Figure S4). These results show the effectiveness of using graphene as a buffer layer to partially decouple the molecular layer from the metallic substrate and avoid on-surface dechlorination of Cl_4TPP molecules. All binding energies (E_{bind}) and full widths at half-maximum (FWHM) of the deconvoluted peaks in our XPS measurements are provided in Table 1.

Next, we study the influence of Cl_4TPP molecules on the electronic properties of graphene/Ir(111) by monitoring the energy-momentum dispersion along the $\overline{\Gamma}\overline{K}$ direction of the Brillouin zone of graphene. Focusing first on the ARPES image of pristine graphene/Ir(111), Figure 2d shows the linear dispersion of graphene π and π^* bands in the vicinity of the Dirac point, where the Dirac cone is slightly shifted below the Fermi level (E_F), due to a marginal p-doping of graphene by the Ir(111) substrate.[43,70−72] Our DFT calculations also show a charge transfer from graphene to Ir(111) of 0.3 electrons per supercell, i.e., −0.07 e/nm^2, consistent with a marginal p-doping of graphene by the Ir(111) substrate. However, simultaneously, the Cl_4TPP molecular overlayer remains completely neutral upon adsorption on graphene/Ir(111) (see Table S1 for Bader charges of Cl_4TPP on graphene/Ir(111)). This further demonstrates that the molecular−substrate interaction is purely via physisorption. A decrease in the photoemission intensity at ≈1.2 eV below E_F is observed (see white arrow in Figure 2d). This faint intensity shows the opening of a minigap in the energy-momentum dispersion of graphene and is reported to be originating from the Moiré pattern of graphene on Ir(111).[43,70,71,73] Last but not least, Figure 2e shows that after deposition of a monolayer of Cl_4TPP molecule on graphene/Ir(111) the intrinsic properties of graphene/Ir(111) are preserved; i.e., the Dirac point remains at ≈0.4 eV below the Fermi level, the Fermi velocity, obtained from the slope of the conical dispersion,[74−76] remains unperturbed, and the minigaps are observed at the same position.

Table 1. Binding Energies E_{bind} and Full Width at Half-Maximum (FWHM) in eV for the XPS Spectra of a Submonolayer of Cl_4TPP Deposited on Graphene/Ir(111)

C 1s	C−C	C−N	C−Cl
E_{bind}	284.50	285.00	285.54
FWHM	0.74	0.54	0.54
N 1s	=N−	−NH−	
E_{bind}	397.95	399.99	
FWHM	1.04	1.04	
Cl 2p	Cl−C	Cl−C	
E_{bind}	202.20	200.59	
FWHM	0.80	0.80	

4. CONCLUSIONS

In summary, we have demonstrated using STM that Cl_4TPP molecules self-assemble on graphene/Ir(111) into a square network, which remains unperturbed, in both periodicity and orientation, by the substrate's step edges, i.e., carpet-like growth. Our DFT relaxed structures show C−Cl···H−C hydrogen bonds mainly stabilize the molecular networks, with a weak hydrogen bond distance of $d_{Cl\cdots H} \approx 2.5$ to 2.9 Å. This yields a Cl_4TPP overlayer binding energy on graphene/Ir(111) of 0.37 eV/molecule relative to the overlayer in gas phase, consistent with a relatively weak physisorption of the molecules on the graphene/Ir(111) surface. Furthermore, we find the Cl_4TPP molecular overlayer remains completely neutral upon adsorption on the graphene/Ir(111). Our experiments show no dechlorination of Cl_4TPP molecules occurs even at temperatures as high as 550 K. Finally, our ARPES and DFT results show no change in the intrinsic electronic properties of pristine graphene. These results not only highlight graphene's potential as a general templating material to decouple highly reactive self-assembled 2D overlayers from a metallic substrate but also show the preservation of pristine graphene's electronic properties.

https://doi.org/10.1021/acs.jpcc.3c00235
J. Phys. Chem. C 2023, 127, 8751−8758

■ ASSOCIATED CONTENT

Supporting Information

The Supporting Information is available free of charge at https://pubs.acs.org/doi/10.1021/acs.jpcc.3c00235.

Additional STM images and XPS spectra; atomic coordinates, Bader charges, and total energy for Cl_4TPP adsorbed on graphene/Ir(111) (PDF)

■ AUTHOR INFORMATION

Corresponding Authors

Abner de Siervo − *Instituto de Física Gleb Wataghin, Universidade Estadual de Campinas, 13083-859 Campinas, SP, Brazil;* orcid.org/0000-0002-7192-4740; Email: asiervo@ifi.unicamp.br

Juan Carlos Moreno-López − *Faculty of Physics, University of Vienna, 1090 Vienna, Austria;* orcid.org/0000-0003-1078-8607; Email: juan.moreno@univie.ac.at

Authors

Duncan John Mowbray − *School of Physical Sciences and Nanotechnology, Yachay Tech University, 100119 Urcuquí, Ecuador;* orcid.org/0000-0002-8520-0364

Alejandro Pérez Paz − *Chemistry Department, United Arab Emirates University, Al Ain, United Arab Emirates;* orcid.org/0000-0003-0959-7184

Rodrigo C. C. Ferreira − *Institute of Physics, Czech Academy of Sciences, Praha 6 CZ16200, Czech Republic*

Valeria Milotti − *Faculty of Physics, University of Vienna, 1090 Vienna, Austria;* orcid.org/0000-0003-4732-1226

Pedro Schio − *Laboratorio Nacional de Luz Sincrotron, Centro Nacional de Pesquisa em Energia e Materiais, 13083-970 Campinas, SP, Brazil*

Wendell Simoes e Silva − *Laboratorio Nacional de Luz Sincrotron, Centro Nacional de Pesquisa em Energia e Materiais, 13083-970 Campinas, SP, Brazil*

Thomas Pichler − *Faculty of Physics, University of Vienna, 1090 Vienna, Austria;* orcid.org/0000-0001-5377-9896

Complete contact information is available at: https://pubs.acs.org/10.1021/acs.jpcc.3c00235

Notes

The authors declare no competing financial interest.

■ ACKNOWLEDGMENTS

J.C.M.L. thanks Prof. Byung-Chul Han for sharing his ideas about self-exploitation laborers, which, unfortunately, are disturbingly true in Academia. The authors thank the Brazilian Synchrotron Light Laboratory (LNLS) and the support of the PGM Beamline scientists to our proposal number PGM-20170630. For calculations we have employed the Imbabura cluster of Yachay Tech University, which was purchased under Contract 2017-024 (SIE-UITEY-007-2017). A.P.P. thanks UAEU for an internal start-up grant (No. 31S410). This work has financial support from Fundação de Amparo a Pesquisa do Estado de São Paulo (FAPESP) under Projects 2007/08244-5, 2007/54829-5, and 2017/18574-4 and from Conselho Nacional Científico e Tecnológico (CNPq) from Brazil..

■ REFERENCES

(1) Valli, A.; Amaricci, A.; Brosco, V.; Capone, M. Quantum interference assisted spin filtering in graphene nanoflakes. *Nano Lett.* **2018**, *18*, 2158−2164.

(2) Muñoz-Rojas, F.; Fernández-Rossier, J.; Palacios, J. Giant magnetoresistance in ultrasmall graphene based devices. *Phys. Rev. Lett.* **2009**, *102*, 136810.

(3) Gani, M.; Shah, K. A.; Parah, S. A.; Misra, P. Room temperature high Giant Magnetoresistance graphene based spin valve and its application for realization of logic gates. *Phys. Lett. A* **2020**, *384*, 126171.

(4) Huang, H.; Zheng, A.; Gao, G.; Yao, K. Thermal spin filtering effect and giant magnetoresistance of half-metallic graphene nanoribbon co-doped with non-metallic Nitrogen and Boron. *J. Magn. Magn. Mater.* **2018**, *449*, 522−529.

(5) Sensale-Rodriguez, B.; Yan, R.; Kelly, M. M.; Fang, T.; Tahy, K.; Hwang, W. S.; Jena, D.; Liu, L.; Xing, H. G. Broadband graphene terahertz modulators enabled by intraband transitions. *Nat. Commun.* **2012**, *3*, 1−7.

(6) Zhang, Y.; Feng, Y.; Zhu, B.; Zhao, J.; Jiang, T. Graphene based tunable metamaterial absorber and polarization modulation in terahertz frequency. *Opt. Express* **2014**, *22*, 22743−22752.

(7) Chen, Z.; Chen, X.; Tao, L.; Chen, K.; Long, M.; Liu, X.; Yan, K.; Stantchev, R. I.; Pickwell-MacPherson, E.; Xu, J.-B. Graphene controlled Brewster angle device for ultra broadband terahertz modulation. *Nat. Commun.* **2018**, *9*, 1−7.

(8) Wu, Y.; Lin, Y.-m.; Bol, A. A.; Jenkins, K. A.; Xia, F.; Farmer, D. B.; Zhu, Y.; Avouris, P. High-frequency, scaled graphene transistors on diamond-like carbon. *Nature* **2011**, *472*, 74−78.

(9) Tong, J.; Conte, M. C.; Goldstein, T.; Yngvesson, S. K.; Bardin, J. C.; Yan, J. Asymmetric two-terminal graphene detector for broadband radiofrequency heterodyne-and self-mixing. *Nano Lett.* **2018**, *18*, 3516−3522.

(10) Wu, Y.; Jenkins, K. A.; Valdes-Garcia, A.; Farmer, D. B.; Zhu, Y.; Bol, A. A.; Dimitrakopoulos, C.; Zhu, W.; Xia, F.; Avouris, P.; et al. State-of-the-art graphene high-frequency electronics. *Nano Lett.* **2012**, *12*, 3062−3067.

(11) Han, S.-J.; Jenkins, K. A.; Valdes Garcia, A.; Franklin, A. D.; Bol, A. A.; Haensch, W. High-frequency graphene voltage amplifier. *Nano Lett.* **2011**, *11*, 3690−3693.

(12) El Abbassi, M.; Sangtarash, S.; Liu, X.; Perrin, M. L.; Braun, O.; Lambert, C.; van der Zant, H. S. J.; Yitzchaik, S.; Decurtins, S.; Liu, S.-X.; et al. Robust graphene-based molecular devices. *Nat. Nanotechnol.* **2019**, *14*, 957−961.

(13) Mol, J. A.; Lau, C. S.; Lewis, W. J.; Sadeghi, H.; Roche, C.; Cnossen, A.; Warner, J. H.; Lambert, C. J.; Anderson, H. L.; Briggs, G. A. D. Graphene-porphyrin single-molecule transistors. *Nanoscale* **2015**, *7*, 13181−13185.

(14) Yang, C.; Qin, A.; Tang, B. Z.; Guo, X. Fabrication and functions of graphene−molecule−graphene single-molecule junctions. *J. Chem. Phys.* **2020**, *152*, 120902.

(15) Wickenburg, S.; Lu, J.; Lischner, J.; Tsai, H.-Z.; Omrani, A. A.; Riss, A.; Karrasch, C.; Bradley, A.; Jung, H. S.; Khajeh, R.; et al. Tuning charge and correlation effects for a single molecule on a graphene device. *Nat. Commun.* **2016**, *7*, 1−7.

(16) Li, J.; Friedrich, N.; Merino, N.; de Oteyza, D. G.; Peña, D.; Jacob, D.; Pascual, J. I. Electrically addressing the spin of a magnetic porphyrin through covalently connected graphene electrodes. *Nano Lett.* **2019**, *19*, 3288−3294.

(17) Barja, S.; Garnica, M.; Hinarejos, J. J.; de Parga, A. L. V.; Martín, N.; Miranda, R. Self-organization of electron acceptor molecules on graphene. *Chem. Commun.* **2009**, *46*, 8198−8200.

(18) Li, J.; Solianyk, L.; Schmidt, N.; Baker, B.; Gottardi, S.; Moreno Lopez, J. C.; Enache, M.; Monjas, L.; van der Vlag, R.; Havenith, R. W.; et al. Low-dimensional metal−organic coordination structures on graphene. *J. Phys. Chem. C* **2019**, *123*, 12730−12735.

(19) Li, J.; Gottardi, S.; Solianyk, L.; Moreno-López, J. C.; Stöhr, M. 1, 3, 5-benzenetribenzoic acid on Cu (111) and graphene/Cu (111): A comparative STM study. *J. Phys. Chem. C* **2016**, *120*, 18093−18098.

(20) Tan, Y.-Z.; Yang, B.; Parvez, K.; Narita, A.; Osella, S.; Beljonne, D.; Feng, X.; Müllen, K. Atomically precise edge chlorination of nanographenes and its application in graphene nanoribbons. *Nat. Commun.* **2013**, *4*, 1−7.
(21) Bouša, D.; Luxa, J.; Mazanek, V.; Jankovskỳ, O.; Sedmidubskỳ, D.; Klimova, K.; Pumera, M.; Sofer, Z. Toward graphene chloride: chlorination of graphene and graphene oxide. *RSC Adv.* **2016**, *6*, 66884−66892.
(22) Li, B.; Zhou, L.; Wu, D.; Peng, H.; Yan, K.; Zhou, Y.; Liu, Z. Photochemical chlorination of graphene. *ACS Nano* **2011**, *5*, 5957−5961.
(23) Zhang, L.; Zhou, L.; Yang, M.; Liu, Z.; Xie, Q.; Peng, H.; Liu, Z. Photo-induced free radical modification of graphene. *Small* **2013**, *9*, 1134−1143.
(24) Yang, M.; Zhou, L.; Wang, J.; Liu, Z.; Liu, Z. Evolutionary chlorination of graphene: from charge-transfer complex to covalent bonding and nonbonding. *J. Phys. Chem. C* **2012**, *116*, 844−850.
(25) Vinogradov, N. A.; Simonov, K.; Generalov, A.; Vinogradov, A.; Vyalikh, D.; Laubschat, C.; Mårtensson, N.; Preobrajenski, A. Controllable p-doping of graphene on Ir (111) by chlorination with FeCl3. *J. Condens. Matter Phys.* **2012**, *24*, 314202.
(26) Andersen, M.; Hornekær, L.; Hammer, B. Understanding intercalation structures formed under graphene on Ir (111). *Phys. Rev. B* **2014**, *90*, 155428.
(27) Miyazaki, H.; Matsumoto, R.; Katagiri, M.; Yoshida, T.; Ueno, K.; Sakai, T.; Kajita, A. MoCl5 intercalation doping and oxygen passivation of submicrometer-sized multilayer graphene. *Jpn. J. Appl. Phys.* **2017**, *56*, 04CP02.
(28) Wang, S.; Yu, J. Bandgap modulation of partially chlorinated graphene (C4Cl) nanosheets via biaxial strain and external electric field: a computational study. *Appl. Phys. A: Mater. Sci. Process.* **2018**, *124*, 1−9.
(29) Sahin, H.; Ciraci, S. Chlorine adsorption on graphene: Chlorographene. *J. Phys. Chem. C* **2012**, *116*, 24075−24083.
(30) Sreeprasad, T.; Berry, V. How do the electrical properties of graphene change with its functionalization? *small* **2013**, *9*, 341−350.
(31) Zhan, D.; Yan, J.; Lai, L.; Ni, Z.; Liu, L.; Shen, Z. Engineering the electronic structure of graphene. *Adv. Mater.* **2012**, *24*, 4055−4069.
(32) Larciprete, R.; Ulstrup, S.; Lacovig, P.; Dalmiglio, M.; Bianchi, M.; Mazzola, F.; Hornekær, L.; Orlando, F.; Baraldi, A.; Hofmann, P.; et al. Oxygen switching of the epitaxial graphene−metal interaction. *ACS Nano* **2012**, *6*, 9551−9558.
(33) Chung, W.-H.; Tsai, D.-S.; Fan, L.-J.; Yang, Y.-W.; Huang, Y.-S. Surface oxides of Ir (111) prepared by gas-phase oxygen atoms. *Surface science* **2012**, *606*, 1965−1971.
(34) Nie, S.; Walter, A. L.; Bartelt, N. C.; Starodub, E.; Bostwick, A.; Rotenberg, E.; McCarty, K. F. Growth from below: graphene bilayers on Ir (111). *ACS Nano* **2011**, *5*, 2298−2306.
(35) Horcas, I.; Fernández, R.; Gomez-Rodriguez, J.; Colchero, J.; Gómez-Herrero, J.; Baro, A. WSXM: a software for scanning probe microscopy and a tool for nanotechnology. *Rev. Sci. Instrum.* **2007**, *78*, 013705.
(36) Cezar, J.; Fonseca, P.; Rodrigues, G.; De Castro, A.; Neuenschwander, R.; Rodrigues, F.; Meyer, B.; Ribeiro, L.; Moreira, A.; Piton, J.; et al. The U11 PGM beam line at the Brazilian national synchrotron Light laboratory. *J. Phys. Conf. Ser.* **2013**, *425*, 072015.
(37) de Campos Ferreira, R. C.; de Lima, L. H.; Barreto, L.; Silva, C. C.; Landers, R.; de Siervo, A. Unraveling the atomic structure of Fe intercalated under graphene on Ir (111): A Multitechnique Approach. *Chem. Mater.* **2018**, *30*, 7201−7210.
(38) Lacovig, P.; Pozzo, M.; Alfe, D.; Vilmercati, P.; Baraldi, A.; Lizzit, S. Growth of dome-shaped carbon nanoislands on Ir (111): the intermediate between carbidic clusters and quasi-free-standing graphene. *Phys. Rev. Lett.* **2009**, *103*, 166101.
(39) Hüfner, S.; Wertheim, G. Core-line asymmetries in the X-ray photoemission spectra of metals. *Phys. Rev. B* **1975**, *11*, 678.
(40) Granas, E.; Knudsen, J.; Schröder, U. A.; Gerber, T.; Busse, C.; Arman, M. A.; Schulte, K.; Andersen, J. N.; Michely, T. Oxygen intercalation under graphene on Ir (111): energetics, kinetics, and the role of graphene edges. *ACS Nano* **2012**, *6*, 9951−9963.
(41) Shirley, D. A. High-resolution X-ray photoemission spectrum of the valence bands of gold. *Phys. Rev. B* **1972**, *5*, 4709.
(42) Starodub, E.; Bostwick, A.; Moreschini, L.; Nie, S.; El Gabaly, F.; McCarty, K. F.; Rotenberg, E. In-plane orientation effects on the electronic structure, stability, and Raman scattering of monolayer graphene on Ir (111). *Phys. Rev. B* **2011**, *83*, 125428.
(43) Ulstrup, S.; Andersen, M.; Bianchi, M.; Barreto, L.; Hammer, B.; Hornekær, L.; Hofmann, P. Sequential oxygen and alkali intercalation of epitaxial graphene on Ir (111): enhanced many-body effects and formation of pn-interfaces. *2D Materials* **2014**, *1*, 025002.
(44) Larsen, A. H.; Vanin, M.; Mortensen, J. J.; Thygesen, K. S.; Jacobsen, K. W. Localized Atomic Basis Set in the Projector Augmented Wave Method. *Phys. Rev. B: Condens. Matter Mater. Phys.* **2009**, *80*, 195112.
(45) Mortensen, J. J.; Hansen, L. B.; Jacobsen, K. W. Real-Space Grid Implementation of the Projector Augmented Wave Method. *Phys. Rev. B: Condens. Matter Mater. Phys.* **2005**, *71*, 035109.
(46) Enkovaara, J.; Rostgaard, C.; Mortensen, J. J.; Chen, J.; Dułak, M.; Ferrighi, L.; Gavnholt, J.; Glinsvad, C.; Haikola, V.; Hansen, H. A.; et al. Electronic Structure Calculations with GPAW: A Real-Space Implementation of the Projector Augmented-Wave Method. *J. Phys.: Condens. Matter* **2010**, *22*, 253202.
(47) Perdew, J. P.; Burke, K.; Ernzerhof, M. Generalized Gradient Approximation Made Simple. *Phys. Rev. Lett.* **1996**, *77*, 3865.
(48) Grimme, S.; Antony, J.; Ehrlich, S.; Krieg, H. A consistent and accurate ab initio parametrization of density functional dispersion correction (DFT-D) for the 94 elements H-Pu. *J. Chem. Phys.* **2010**, *132*, 154104.
(49) de Campos Ferreira, R. C.; Pérez Paz, A.; Mowbray, D. J.; Roulet, J.-Y.; Landers, R.; de Siervo, A. Supramolecular ordering and reactions of a chlorophenyl porphyrin on Ag(111). *J. Phys. Chem. C* **2020**, *124*, 14220−14228.
(50) Bader, R. F. W. *Atoms in Molecules: A Quantum Theory*; Oxford University: 1990; Vol. 3, pp 1−120.
(51) Tang, W.; Sanville, E.; Henkelman, G. A grid-based Bader analysis algorithm without lattice bias. *J. Phys.: Condens. Matter* **2009**, *21*, 084204.
(52) Tersoff, J.; Hamann, D. R. Theory of the scanning tunneling microscope. *Phys. Rev. B* **1985**, *31*, 805−813.
(53) Larsen, A. H.; Mortensen, J. J.; Blomqvist, J.; Castelli, I. E.; Christensen, R.; Dułak, M.; Friis, J.; Groves, M. N.; Hammer, B.; Hargus, C.; et al. The atomic simulation environment—a Python library for working with atoms. *J. Phys.: Condens. Matter* **2017**, *29*, 273002.
(54) Coraux, J.; N'Diaye, A. T.; Busse, C.; Michely, T. Structural coherency of graphene on Ir (111). *Nano Lett.* **2008**, *8*, 565−570.
(55) N'Diaye, S.; Bleikamp, A. T.; Feibelman, P. J.; Michely, T. Two-dimensional Ir cluster lattice on a graphene moiré on Ir (111). *Phys. Rev. Lett.* **2006**, *97*, 215501.
(56) Standop, S.; Lehtinen, O.; Herbig, C.; Lewes-Malandrakis, G.; Craes, F.; Kotakoski, J.; Michely, T.; Krasheninnikov, A. V.; Busse, C. Ion impacts on graphene/Ir (111): interface channeling, vacancy funnels, and a nanomesh. *Nano Lett.* **2013**, *13*, 1948−1955.
(57) Moreno-López, J. C.; Mowbray, D. J.; Perez Paz, A.; de Campos Ferreira, R. C.; Ceccatto dos Santos, A.; Ayala, P.; de Siervo, A. Roles of precursor conformation and adatoms in ullmann coupling: An inverted porphyrin on Cu (111). *Chem. Mater.* **2019**, *31*, 3009−3017.
(58) Tersoff, J.; Hamann, D. R. Theory and application for the scanning tunneling microscope. *Physical review letters* **1983**, *50*, 1998.
(59) Busse, C.; Lazić, P.; Djemour, R.; Coraux, J.; Gerber, T.; Atodiresei, N.; Caciuc, V.; Brako, R.; Blügel, S.; Zegenhagen, J.; et al. Graphene on Ir (111): physisorption with chemical modulation. *Physical review letters* **2011**, *107*, 036101.
(60) Barreto, L.; de Lima, L. H.; Martins, D. C.; Silva, C.; de Campos Ferreira, R. C.; Landers, R.; de Siervo, A. Selecting

https://doi.org/10.1021/acs.jpcc.3c00235
J. Phys. Chem. C 2023, 127, 8751−8758

'convenient observers' to probe the atomic structure of CVD graphene on Ir (111) via photoelectron diffraction. *J. Phys.: Condens. Matter* **2021**, *33*, 105001.
(61) Auwärter, W.; Écija, D.; Klappenberger, F.; Barth, J. V. Porphyrins at interfaces. *Nat. Chem.* **2015**, *7*, 105−120.
(62) Mielke, J.; Hanke, F.; Peters, M. V.; Hecht, S.; Persson, M.; Grill, L. Adatoms underneath single porphyrin molecules on Au (111). *J. Am. Chem. Soc.* **2015**, *137*, 1844−1849.
(63) Jarvis, S. P.; Taylor, S.; Baran, J. D.; Thompson, D.; Saywell, A.; Mangham, B.; Champness, N. R.; Larsson, J.; Moriarty, P. Physisorption controls the conformation and density of states of an adsorbed porphyrin. *J. Phys. Chem. C* **2015**, *119*, 27982−27994.
(64) Lepper, M.; Köbl, J.; Schmitt, T.; Gurrath, M.; de Siervo, A.; Schneider, M. A.; Steinrück, H.-P.; Meyer, B.; Marbach, H.; Hieringer, W. Inverted" porphyrins: a distorted adsorption geometry of free-base porphyrins on Cu (111). *Chem. Commun.* **2017**, *53*, 8207−8210.
(65) Bianchi, M.; Cassese, D.; Cavallin, A.; Comin, R.; Orlando, F.; Postregna, L.; Golfetto, E.; Lizzit, S.; Baraldi, A. Surface core level shifts of clean and oxygen covered Ir (111). *New J. Phys.* **2009**, *11*, 063002.
(66) Klimovskikh, I. I.; Vilkov, O.; Usachov, D. Y.; Rybkin, A.; Tsirkin, S.; Filianina, M.; Bokai, K.; Chulkov, E.; Shikin, A. Variation of the character of spin-orbit interaction by Pt intercalation underneath graphene on Ir (111). *Phys. Rev. B* **2015**, *92*, 165402.
(67) Moulder, J.; Stickle, W. F..; Sobol, P. E.; Bomben, K. D.; Chastain, J. *Handbook of X-ray Photoelectron Spectroscopy*; Perkin−Elmer Corporation: 1992.
(68) Medford, A. J.; Vojvodic, A.; Hummelshøj, J. S.; Voss, J.; Abild-Pedersen, F.; Studt, F.; Bligaard, T.; Nilsson, A.; Nørskov, J. K. From the Sabatier principle to a predictive theory of transition-metal heterogeneous catalysis. *J. Catal.* **2015**, *328*, 36−42.
(69) Pham, V. D.; Lagoute, J.; Mouhoub, O.; Joucken, F.; Repain, V.; Chacon, C.; Bellec, A.; Girard, Y.; Rousset, S. Electronic interaction between nitrogen-doped graphene and porphyrin molecules. *ACS Nano* **2014**, *8*, 9403−9409.
(70) Kralj, M.; Pletikosić, I.; Petrović, M.; Pervan, P.; Milun, M.; Busse, C.; Michely, T.; Fujii, J.; Vobornik, I.; et al. Graphene on Ir (111) characterized by angle-resolved photoemission. *Phys. Rev. B* **2011**, *84*, 075427.
(71) Pletikosić, I.; Kralj, M.; Pervan, P.; Brako, R.; Coraux, J.; N'diaye, A.; Busse, C.; Michely, T. Dirac cones and minigaps for graphene on Ir (111). *Phys. Rev. Lett.* **2009**, *102*, 056808.
(72) Kastorp, C. F.; Duncan, D. A.; Scheffler, M.; Thrower, J. D.; Jørgensen, A. L.; Hussain, H.; Lee, T.-L.; Hornekær, L.; Balog, R. Growth and electronic properties of bi-and trilayer graphene on Ir (111). *Nanoscale* **2020**, *12*, 19776−19786.
(73) Voloshina, E.; Dedkov, Y. Graphene on metallic surfaces: problems and perspectives. *Phys. Chem. Chem. Phys.* **2012**, *14*, 13502−13514.
(74) Siegel, D. A.; Park, C.-H.; Hwang, C.; Deslippe, J.; Fedorov, A. V.; Louie, S. G.; Lanzara, A. Many-body interactions in quasi-freestanding graphene. *Proc. Natl. Acad. Sci. U. S. A.* **2011**, *108*, 11365−11369.
(75) Hicks, J.; Sprinkle, M.; Shepperd, K.; Wang, F.; Tejeda, A.; Taleb-Ibrahimi, A.; Bertran, F.; Le Févre, P.; De Heer, W.; Berger, C.; et al. Symmetry breaking in commensurate graphene rotational stacking: comparison of theory and experiment. *Phys. Rev. B* **2011**, *83*, 205403.
(76) Avila, J.; Razado, I.; Lorcy, S.; Fleurier, R.; Pichonat, E.; Vignaud, D.; Wallart, X.; Asensio, M. C. Exploring electronic structure of one-atom thick polycrystalline graphene films: A nano angle resolved photoemission study. *Sci. Rep.* **2013**, *3*, 2439.

https://doi.org/10.1021/acs.jpcc.3c00235
J. Phys. Chem. C 2023, 127, 8751−8758